Article

An Adaptive Frequency Strategy for Variable Speed Wind Turbines: Application to High Wind Integration Into Power Systems

Ana Fernández-Guillamón [1],* [iD], Jorge Villena-Lapaz [2], Antonio Vigueras-Rodríguez [3] [iD], Tania García-Sánchez [4] and Ángel Molina-García [1] [iD]

[1] Department of Electrical Engineering, Universidad Politécnica de Cartagena, 30202 Cartagena, Spain; angel.molina@upct.es
[2] Alberta Electric System Operator, Calgary, AB T2P 0L4, Canada; jorge.villena@aeso.ca
[3] Department of Civil Engineering, Universidad Politécnica de Cartagena, 30203 Cartagena, Spain; avigueras.rodriguez@upct.es
[4] Department of Electrical Engineering, Universidad Politécnica de Valencia, 46022 Valencia, Spain; tagarsan@die.upv.es
* Correspondence: ana.fernandez@upct.es; Tel.: +34-968-325357

Abstract: This paper presents a new frequency controller for variable speed wind turbines connected to the grid under power imbalance conditions. It is based on the fast power reserve emulation technique, having two different operation modes: overproduction and recovery mode. In the first mode, the active power provided by wind turbines is set over the mechanical power, reducing their rotational speed. This overproduction power is estimated according to the frequency excursion. In the second mode, the active power is established under the mechanical power to recover the initial rotational speed through a smooth trajectory. The power system considered for simulation purposes includes thermal, hydro-power and wind-power plants. The controller proposed has been evaluated under different mix-generation scenarios implemented in Matlab/Simulink. Extensive results and comparison to previous proposals are also included in the paper.

1. Introduction

During the last decade, and due to aspects such as climate change, energy dependence, fossil resource scarcity and the increasing costs of nuclear power [1], most developed countries have promoted large-scale integration of Renewable Energy Sources (RES), mainly wind and PV power plants [2]. This relevant integration of RES has raised important concerns in terms of grid stability and reliability, mainly due to: (i) the nature of RES power variation [3] as well as the uncertainty in the privately-owned renewable generators that puts the generation-load balance at risk [4]; (ii) the reduction of the total system inertia by the decoupling between rotor mechanical speed and grid frequency [5], or even the absence of rotating machines [6]. As the system inertia decreases, an increase of primary frequency control (PFC) reserves is needed [7]. Traditionally, PFC reserves are provided by synchronous generators [8], as depicted in Figure 1a. Under power imbalance conditions, PFC reserves from conventional generation are traditionally released to compensate the disturbance and recover the rate grid frequency. If these reserves cannot compensate for the mismatch, it could cause a sharp decrease of the system frequency [9]. With the relevant penetration of wind power plants, some proportional capacity of the system reserves must be provided by them [7,10] see Figure 1b.

Additional reserves can be then provided by renewables, reducing the primary reserves from conventional generation units and providing enhanced solutions for weak and/or isolated power systems [9,11]. Under this scenario of high RES penetration, transmission system operators have required that not only conventional utilities contribute to ancillary services [12], but also renewables, especially wind power plants [13]. Indeed, [14] affirms that the participation of the wind power plants in the ancillary services such as grid frequency control becomes inevitable. For this reason, frequency control strategies are being developed to effectively integrate Variable Speed Wind Turbines (VSWTs) into the grid, in order to replace conventional power plants by maintaining a secure power system operation [15]. Most of them are based on 'hidden inertia emulation', in order to enhance the inertia response of VSWTs [16,17]. A classification for different control strategies based on principles for inertia emulation concept can be found in [18]. One of the possible solutions to overcome this is called fast power reserve emulation. It is based on supplying the kinetic energy stored in the rotating masses to the grid as an additional active power, being afterwards recovered through an under-production period (recovery). Overproduction is defined in the specific literature over the electrical pre-event power reference [19–24] and the overproduction power is considered as constant and independent from the frequency excursion severity [21–23]. Other proposals define the time that the wind power plant must be overproducing independently from the event [19–22] or consider that it should last until the wind turbine achieves its minimum speed limit [23]. Moreover, the transition from overproduction to recovery is defined as an abrupt drop in the active generated power by VSWTs [21,23,24] or as a constant slope [19,22]. A different strategy is described in [20], where the VSWTs of the wind power plant are designed to recover at different times, avoiding 'synchronization'. Most contributions consider a low wind energy integration for simulations, between 10 and 20% [19,20,22], and only recent contributions analyze penetration level scenarios up to 40% [10]. However, the renewable share is currently over 20% in different power systems. Actually, some countries have already experienced instantaneous penetration higher than 50% (i.e., Spain, Portugal, Ireland, Germany and Denmark) [25]. Subsequently, scenarios with a very relevant integration of wind energy should be considered and evaluated.

To overcome these drawbacks, and with the aim of improving the frequency response of power systems with massive wind energy penetration, this paper describes and evaluates an alternative fast power reserve emulation controller. The main contributions of this paper are summarized as follows:

- The active power provided by VSWTs during the overproduction operation mode is defined over the mechanical power instead of the pre-event electrical power. Such mechanical power varies with the rotational speed instead of keeping constant as the former one. Moreover, the overproduction power is estimated according to the frequency excursion, being thus an 'adaptive' overproduction strategy.
- The active power provided by VSWTs during the recovery operation mode is defined below the mechanical power to recover the rotational energy delivered in the overproduction mode. It is defined as a parabolic trajectory until the rotational speed reaches the maximum power tracking curve. Thereafter, that curve is followed. Because of that, it is considered as a 'smooth' recovery period.
- The control strategy proposed has been tested under different scenarios, considering a maximum wind energy integration of 45%. In all the scenarios, the proposed solution reduces significantly the grid frequency deviations under power imbalance conditions.

The rest of the paper is organized as follows: in Section 2 the proposed frequency controller for VSWTs is described and compared to previous approaches. The power system and the different scenarios needed to assess the proposed control are discussed in Section 3. Simulation results are given in Section 4. Finally, Section 5 gives the conclusions.
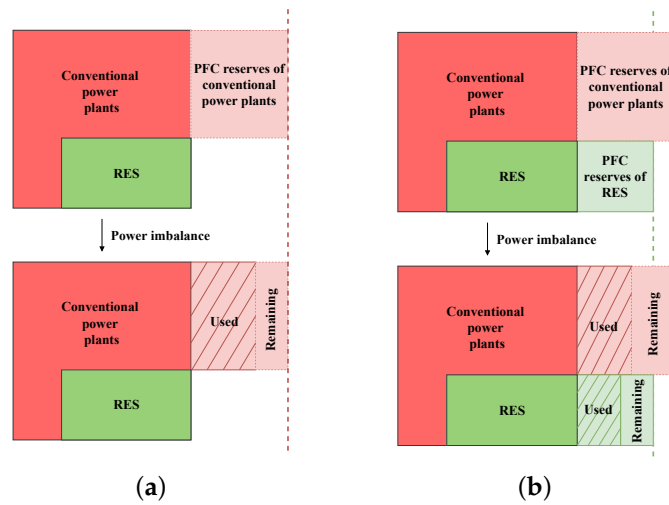
Figure 1. Change in primary frequency control (PFC) reserves from current to future power systems: (**a**) Current situation; (**b**) Future situation.

2. Proposed Frequency Strategy for Wind Turbines

A new frequency control strategy for VSWTs is presented in this work. It is based on supplying the kinetic energy stored in the rotating masses of the VSWT in order to enhance its inertial response. Three different operation modes are defined: normal operation, overproduction mode and recovery mode. Each mode sets a different commanded active power P_{cmd} to restore the grid frequency after a power imbalance. In Figure 2, a general scheme of the proposed VSWTs frequency controller is shown.
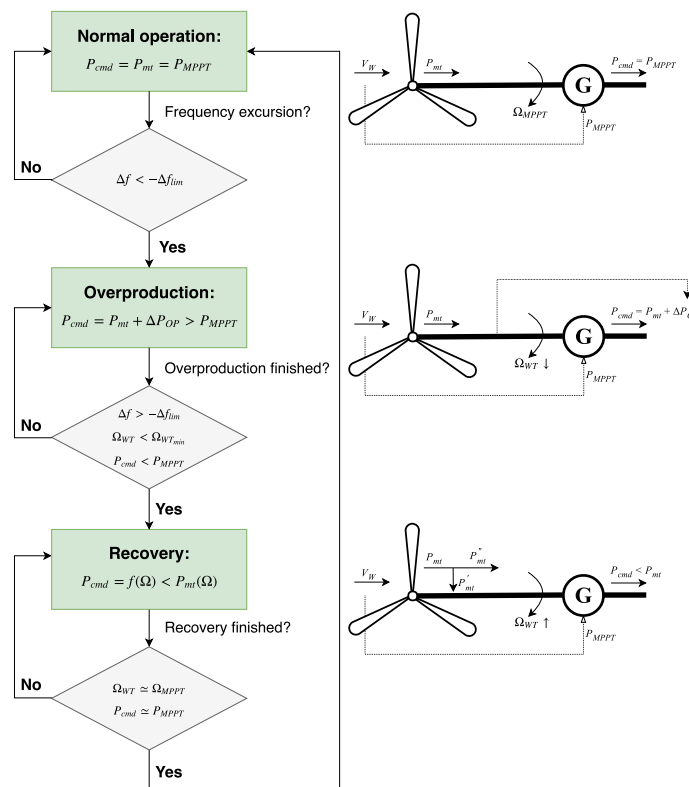

Figure 2. Scheme of the proposed Variable Speed Wind Turbines (VSWTs) frequency controller.

2.1. Normal Operation Mode

The VSWTs operate at a certain point P_{cmd} according to their mechanical curve $P_{mt}(\Omega_{WT})$. The power controller compensates any change in the rotational speed Ω_{WT} or in the wind speed V_W, tracking the maximum available active power for a current wind speed $P_{MPPT}(V_W)$

Under power imbalance conditions, and assuming a power supply-side decreasing, a frequency (negative) deviation Δf is suffered by the power system. The proposed frequency controller is then initialized through an adaptive overproduction strategy:

$$\Delta f < -\Delta f_{lim} \rightarrow \text{Overproduction}.$$

2.2. Overproduction Operation Mode

The active power provided by the VSWTs, P_{cmd}, involves the mechanical power $P_{mt}(\Omega_{WT})$ obtained from the wind and an additional active power ΔP_{OP} taken from the rotational speed energy stored in the rotor, $P_{cmd} = P_{mt}(\Omega_{WT}) + \Delta P_{OP}$. The proposed strategy results in a rotational speed decreasing, and subsequently a reduction of the mechanical power provided by the blades. Regarding to the additional power ΔP_{OP}, it is estimated proportionally to the frequency excursion evolution, see Figure 3, which gives an adaptive response depending on the frequency excursion severity and thus emulating PFC of conventional generation units [26,27]. This strategy gives a more realistic scenario, a smoother response and, additionally, provides a frequency response in line with conventional primary frequency performances. Previous approaches assume the overproduction as a constant value and independent on the frequency excursion [21–23]. Moreover, the overproduction mode defined in this work considers that mechanical power P_{mt} depends on the rotational speed $P_{mt}(\Omega_{WT})$, whereas most authors assumed that mechanical power was constant when rotational speed decreased [19–24]. This overproduction strategy remains active until the frequency excursion disappears, the rotational speed reaches a minimum allowed value, or the commanded power is lower than the maximum available active power.

$$\Delta f > -\Delta f_{lim} \quad \text{or} \quad \Omega_{WT} < \Omega_{WT,min} \quad \text{or} \quad P_{cmd} < P_{MPPT}(\Omega_{MPPT}) \rightarrow \text{Recovery}.$$

In previous contributions, the minimum rotational speed was considered as a constant value; i.e., $\Omega_{WT,min} = 0.7$ pu in [23]. Under this assumption, the rotational speed deviation interval, $\Delta\Omega$ depends on the initial rotational speed value Ω_{MPPT}, giving different regulation ranges. To improve this solution, the minimum rotational speed is proposed to be determined according to the initial value Ω_{MPPT}, being thus $\Omega_{WT,min} = 0.7 \cdot \Omega_{MPPT}$. This way, $\Omega_{WT,min}$ is a function of Ω_{MPPT} and a 30% of rotational speed deviation is allowed. Figure 4a shows the corresponding $\Delta\Omega_{WT} = \Omega_{MPPT} - \Omega_{WT,min}$ differences depending on the wind speed values V_W considering a fixed $\Omega_{WT,min}$. Figure 4b depicts the proposed definition for $\Omega_{WT,min}$. In addition, Figure 5 compares the overproduction strategy discussed in [23] and the alternative approach proposed in this work.
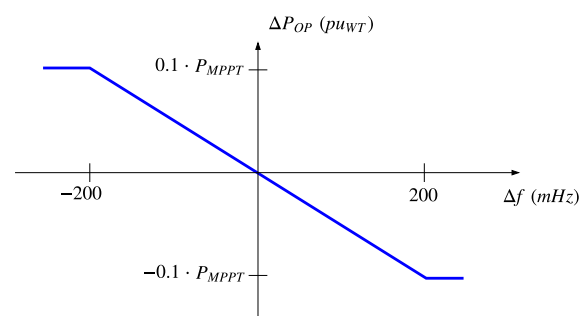

Figure 3. Proposed relationship between ΔP_{OP} and Δf for VSWTs during overproduction.
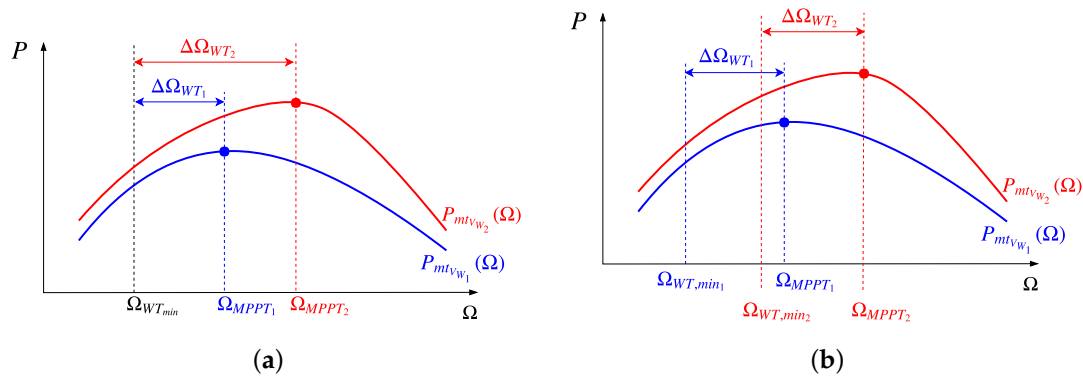
Figure 4. Comparison between overproduction operation modes. (**a**) $\Delta\Omega_{WT}$ for different wind speeds V_W, [23]; (**b**) Proposed $\Delta\Omega_{WT}$ for different wind speeds V_W.
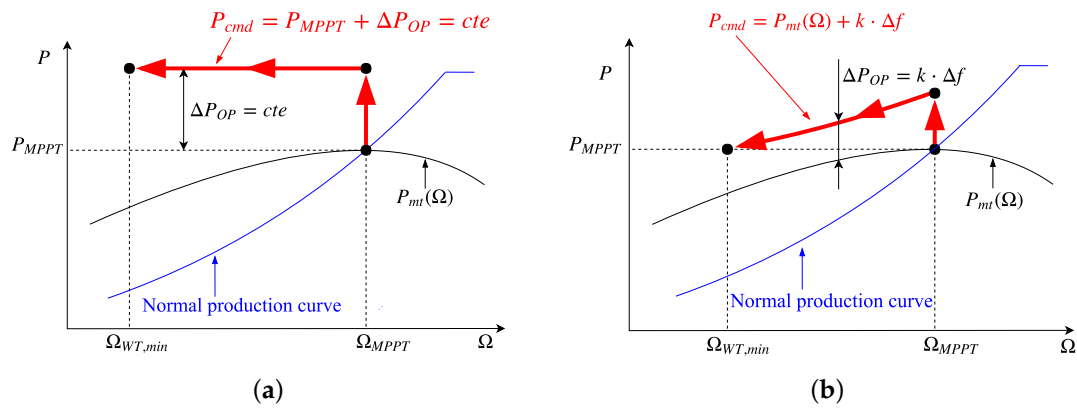

Figure 5. Comparison between overproduction operation modes; (**a**) Overproduction operation mode in [23]; (**b**) Overproduction operation mode proposed.

2.3. Recovery Operation Mode

After the overproduction period, a recovery operation mode is proposed to restore the rotational speed to the initial value Ω_{MPPT} and provide an optimal active power from the VSWTs. With the aim of minimizing undesirable frequency oscillations and abrupt changes from the supply-side, an alternative recovery strategy is defined and evaluated. This proposal is based on a parabolic smooth recovery strategy. Three points are considered to define this trajectory: (i) mechanical power at the minimum rotational speed achieved during the frequency excursion,

$$P_1 : (\Omega_{WT,min}, \ P_{mt}(\Omega_{WT,min}))$$

(ii) mechanical power corresponding to the middle rotational speed deviation,

$$P_2 : (\Omega_V, \ P_{MPPT}(\Omega_V)),$$

where Ω_V is $\Omega_{WT,min} + 0.5 \cdot \Delta\Omega$, and $\Delta\Omega$ is $\Omega_{MPPT} - \Omega_{WT,min}$. (iii) maximum mechanical power available according to the wind speed,

$$P_3 : (\Omega_{MPPT}, \ P_{MPPT}(\Omega_{MPPT})).$$

The commanded power before achieving P_2 is determined according to $P_{cmd} = a \cdot \Omega_{WT}^2 + b \cdot \Omega_{WT} + c$, where a, b and c can be estimated by considering the three mechanical power points aforementioned. Finally, the commanded power tracks the maximum power curve available according to the power wind speed curve: $P_{cmd} = P_{MPPT}(\Omega_{WT})$. The normal operation mode is then recovered when either Ω_{MPPT} or $P_{MPPT}(\Omega_{MPPT})$ are respectively achieved,

$$\Omega_{WT} \simeq \Omega_{MPPT} \quad \text{or} \quad P_{cmd} \simeq P_{MPPT}(\Omega_{MPPT}) \rightarrow \text{Normal operation.}$$

In [23] the recovery period is defined as $P_{cmd} = P_{mt} - P_{acc}$, being P_{acc} a constant underproduction power value. Under this assumption, the higher P_{acc}, the faster the rotational speed recovers its optimal initial value Ω_{MPPT}. Despite the fact that a value of $P_{acc} = 0.02$ pu was fixed, the fast and abrupt transition from overproduction to recovery operation mode may cause an additional and severe frequency oscillation. The recovery operation mode defined in this work determines the trajectory followed by the wind farm instead of fixing a certain underproduction power, P_{acc}. In Figure 6, a comparison between the recovery mode proposed in [23] and the alternative strategy described in this work is depicted. Furthermore, the recovery operation mode has been improved by modifying P_2. The power in point P_2 is then defined in accordance to the differences between $P_{MPPT}(\Omega_V)$ and $P_{mt}(\Omega_V)$, $P_{MPPT}(\Omega_V) + x \cdot (P_{mt}(\Omega_V) - P_{MPPT}(\Omega_V))$, where x has been considered as 0.25, 0.50 and 0.75. When P_{cmd} achieves P_{2_x}, the active power is above the curve of P_{MPPT} proportionally to the difference between $P_{mt}(\Omega_{WT})$ and $P_{MPPT}(\Omega_{WT})$, providing an adaptive and smooth recovery response. In Figure 7, the different proposals for the recovery operation mode are compared.
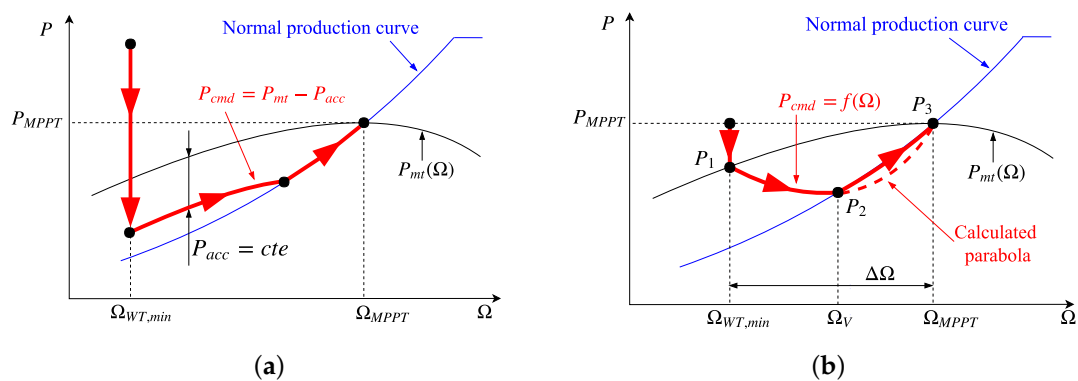

Figure 6. Comparison between recovery operation modes. (**a**) Recovery operation mode in [23]; (**b**) Recovery operation mode proposed.
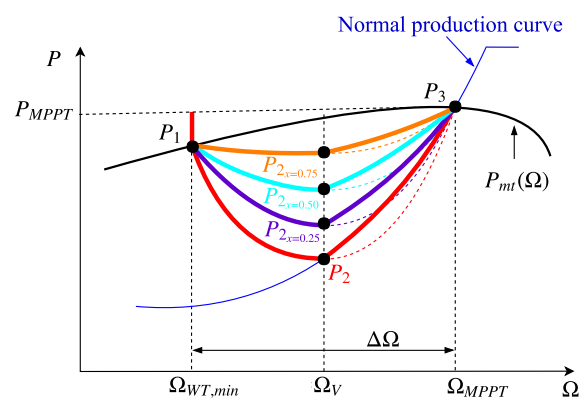

Figure 7. Different proposals for recovery operation mode.

In Figure 8a, the control strategy proposed in [23] is shown. Figure 8b summarizes the new approach discussed in this work. Moreover, Figure 9 compares the VSWTs active power variations submitted to a frequency excursion, where $\Delta P_{WF} = P_{cmd} - P_{MPPT}(\Omega_{MPPT})$. As can be seen, the proposed strategy offers a more adaptive and smoother power oscillation, which leads to reduce possible frequency oscillations due to abrupt imbalances.
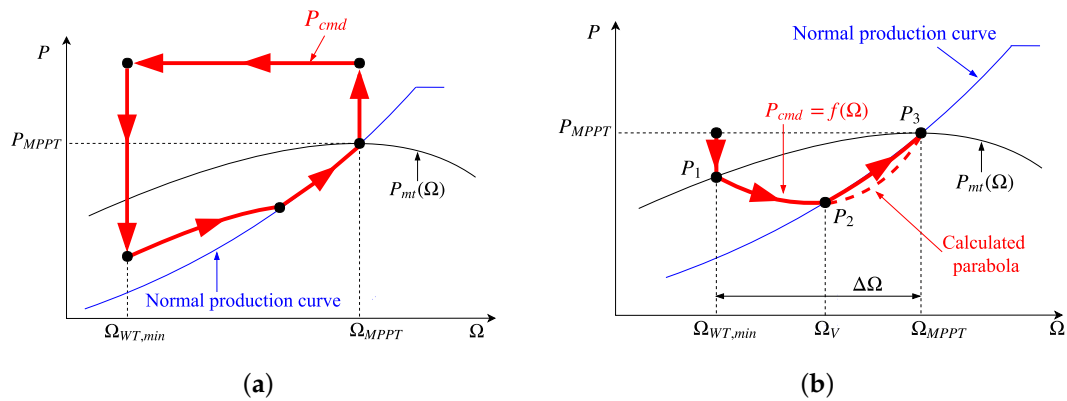

Figure 8. Comparison of frequency control strategies for VSWT. (**a**) Control strategy in [23]; (**b**) Adaptive and smooth proposed control strategy.
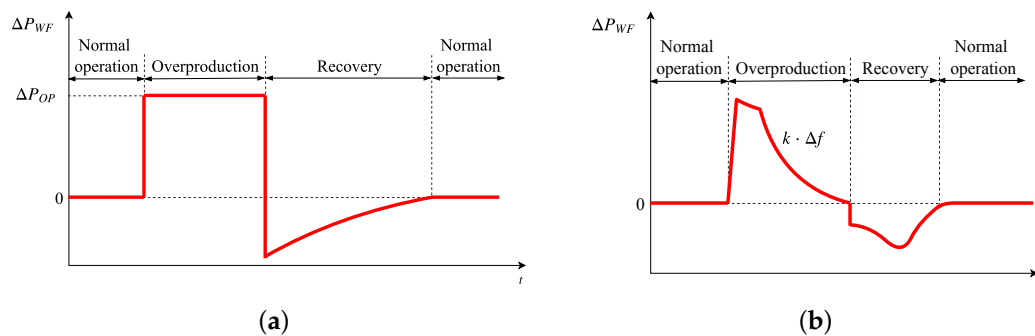

Figure 9. Additional active power of wind power plants: comparison of strategies. (**a**) ΔP_{WF} in [23]; (**b**) ΔP_{WF} proposed.

3. Cases of Study

3.1. Power System Modeling

From the supply-side, the power system considered for simulation purposes involve conventional generating units such as thermal and hydro-power plants, and wind power plants, Simulations have been carried out in Matlab/Simulink. The total capacity of the power system is 1350 MW. Simplified governor-based models have been used to simulate both thermal and hydro-power plants according to [26], see Figure 10a,b. In Appendix A, the different values of the parameters of the block diagrams are presented. To simulate the wind power plant, an equivalent generator with n-times the nominal power of one wind turbine is assumed [28], being n the total number of turbines [29,30]. The frequency controller introduced in Section 2 is added to the wind power plant model in order to provide frequency response under power imbalances. With those considerations, the block diagram of the VSWT can be seen in Figure 10c. Appendix B explains the different blocks of the VSWT model.
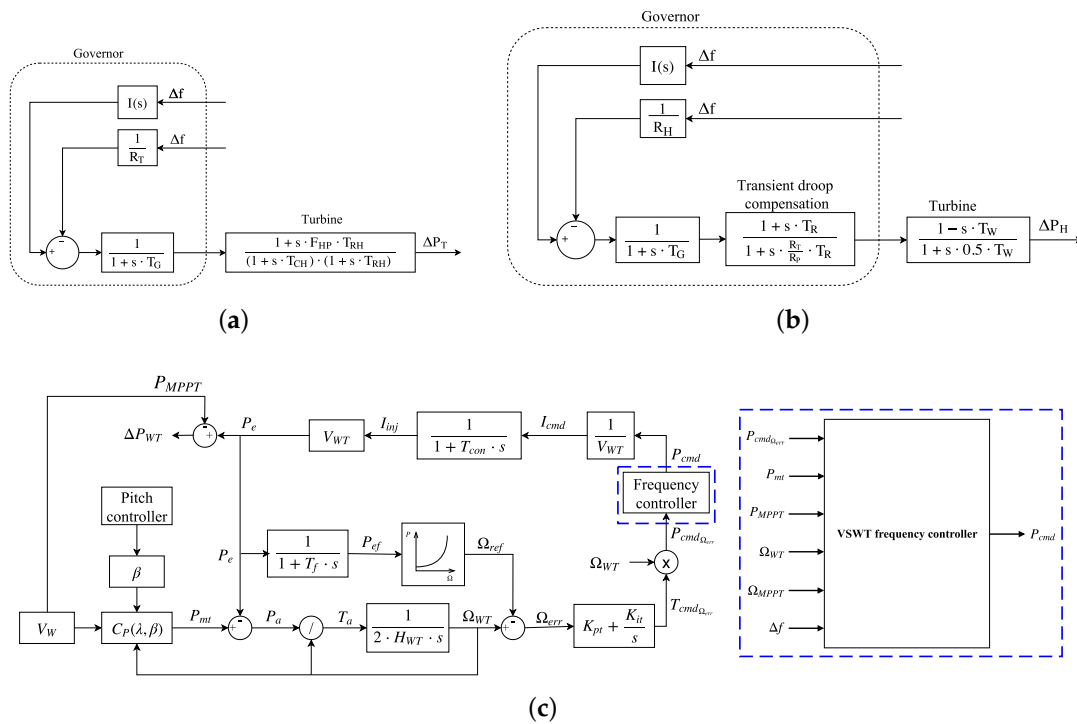
Figure 10. Power plants models. (**a**) Block diagram of a thermal plant model; (**b**) Block diagram of a hydro-power plant model; (**c**) Block diagrams of a VSWT model and the proposed frequency controller.

A simplified diagram in terms of variations of the power system can be seen in Figure 11, being the generated extra power $\Delta P_g = \Delta P_{WF} + \Delta P_T + \Delta P_H$ (the sum of the active power variation of the wind power, thermal and hydro-power plants), and ΔP_L the demand variation. The frequency excursion can be thus estimated from the following expression,

$$\Delta f = \frac{1}{2\,H_{eq}\,s + D_{eq}} \cdot (\Delta P_g - \Delta P_L), \tag{1}$$

where D_{eq} is the equivalent damping factor of the loads and H_{eq} is the equivalent inertia constant of the system, determined as Equation (2)

$$H_{eq} = \frac{\sum_{i=1}^{N} H_i \cdot S_{B,i}}{S_B}, \tag{2}$$

H_i refers to the inertia constant of power plant i, $S_{B,i}$ is the rated power of power plant i, S_B is the rated power of the power system and N is the total number of conventional generators.
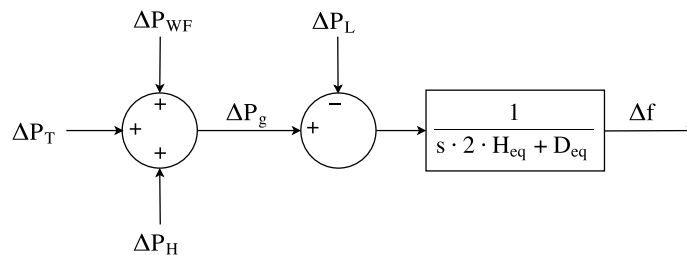

Figure 11. Simplified diagram of the modeled power system.

3.2. Description of the Scenarios

Taking into account the contribution of the different sources from the supply-side in the EU-28 during 2016, see Table 1, four different scenarios have been studied. The first scenario corresponds to the current European supply-side situation, where 75% comes from thermal power plants (conventional and nuclear plants), 12% from hydro-power plants and 13% from non-manageable sources, mainly wind, and other renewables that do not provide frequency control. According to the relevant presence of wind energy, in the rest of scenarios the non-manageable sources have been considered to be just wind power plants. Moreover, the frequency controllers indicated in Section 2 (approach of [23] and the new scheme proposed in this work) have been included in the wind power plant model, keeping constant the capacity of the hydro-power plant (12%). Both thermal and wind capacities have changed depending on the scenarios in order to simulate a power system with high integration of RES. As a consequence, the total inertia of the power system is reduced, due to the fact that VSWTs and thus wind power plants are decoupled from the grid. The considered scenarios for simulation purposes are summarized in Table 2, where H_{eq} has been determined according to Equation (2). To evaluate the VSWTs frequency controller, three power imbalances ($\Delta P_{L,1} = 0.025$, $\Delta P_{L,2} = 0.050$, $\Delta P_{L,3} = 0.100$) have been considered, resulting in 12 different scenarios.

Table 1. Contribution of sources in EU-28 in 2016 [31].

Source	Contribution (%)
Conventional thermal	48.6
Nuclear	25.8
Hydro	12.0
Wind	9.7
Geothermal	0.2
Other	3.7

Table 2. Capacity of each generating unit and total RES integration.

Source	Scenario 1	Scenario 2	Scenario 3	Scenario 4
Thermal plant	75%	73%	58%	43%
Hydro-power plant	12%	12%	12%	12%
Wind power plant	Others	15%	30%	45%
H_{eq}	4.15 s	4.05 s	3.29 s	2.54 s

4. Results

With the aim of evaluating the suitability of the proposed VSWTs frequency controller, three different strategies have been analyzed:

1. Thermal and hydro-power plants with frequency control (without frequency response from wind power plants).
2. Thermal and hydro-power plants with frequency control and wind power plants with the frequency controller of [23].
3. Thermal and hydro-power plants with frequency control and wind power plants with the proposed frequency controller.

When wind power plants are excluded from frequency control, frequency excursions by considering the different scenarios are shown in Figure 12. As wind power integration increases, without providing frequency response, the lowest point or Nadir becomes more and more significant,

achieving -302 mHz in scenario 4 considering the same value of ΔP_L, being over 1.5 times in comparison to the first one. With regard to the stabilization time (defined as the time interval taken by the frequency deviation to be within the range $|\Delta f| < 10$ mHz [32]), it enhances slightly. In scenario 4, it is 1.3 times over the first one, increasing from 28 to 34 s. The rate of change of frequency (ROCOF) also increases with the integration of wind energy without frequency response, from 83 mHz/s in scenario 1 to 132 mHz/s in scenario 4. Therefore, the more wind power integration into grids, the more sensitive is the power system under imbalance conditions. Subsequently, a more unstable grid results from the integration of renewables without implementing any frequency response. Similar relationships are found when $\Delta P_L = 0.050$ and $\Delta P_L = 0.100$ (Figure 12b,c, respectively). In Figure 13, a comparison among Nadir, stabilization time and ROCOF for the different scenarios and $\Delta P_L = 0.050$ is depicted. Results are shown in pu, considering as base the results of scenario 1, where there are no wind power plants.
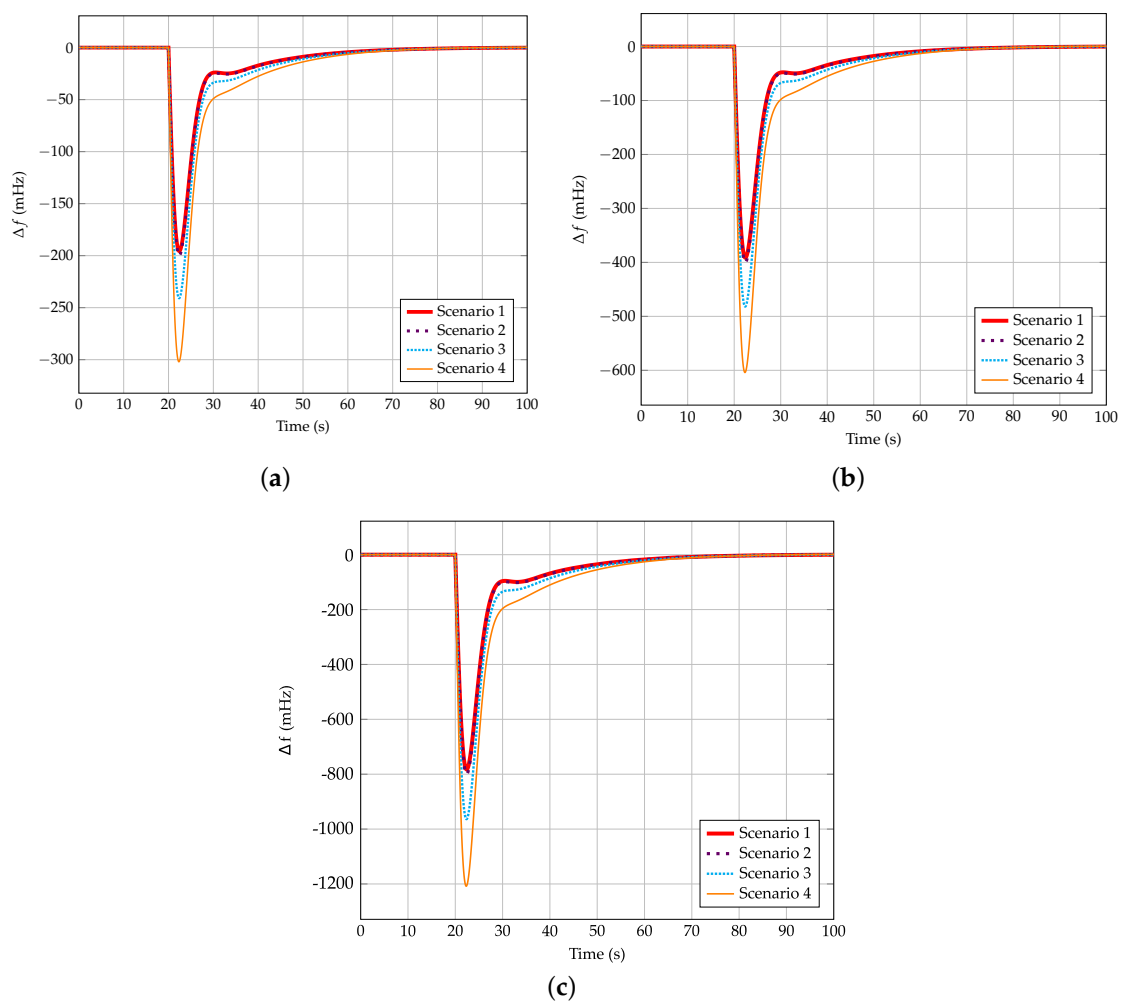

Figure 12. Frequency excursions for scenarios 1–4 without wind power plant control. (**a**) Considering $\Delta P_L = 0.025$; (**b**) Considering $\Delta P_L = 0.050$; (**c**) Considering $\Delta P_L = 0.100$.

To overcome previous frequency excursion drawbacks, and to determine the most suitable recovery strategy of the smooth controller proposed in this work, the four different recovery strategies are analyzed hereinafter. They are represented for the scenario 2, considering $\Delta P_L = 0.050$ in Figure 14a and $\Delta P_L = 0.100$ in Figure 14b. Due to the low value of the power of point P_2 (see Figure 7), the frequency deviation presents undesirable oscillations when the wind power plant is within the

recovery operation mode. This effect is especially significant in the original proposal, and it is reduced as the power considers the difference between the actual mechanical power $P_{mt}(\Omega_{WT})$ and the maximum mechanical power available according to the wind speed $P_{MPPT}(\Omega_{WT})$. Actually, the best response is obtained when P_2 is defined as $P_{MPPT}(\Omega_V) + 0.75 \cdot (P_{mt}(\Omega_{WT}) - P_{MPPT}(\Omega_{WT}))$. Because of that, the rest of the results only consider that case ($x = 0.75$).
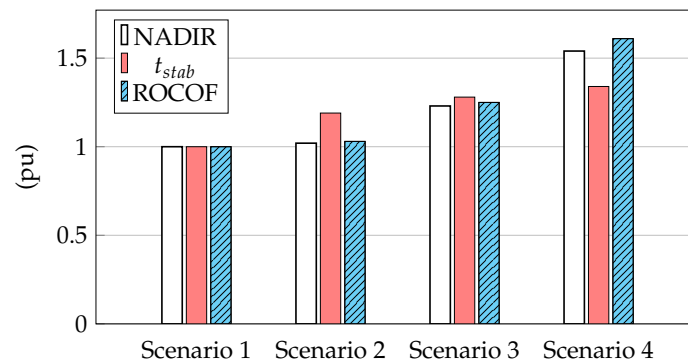

Figure 13. Nadir, stabilization time and the rate of change of frequency (ROCOF): comparison for the different scenarios without wind power plant control for $\Delta P_L = 0.050$.
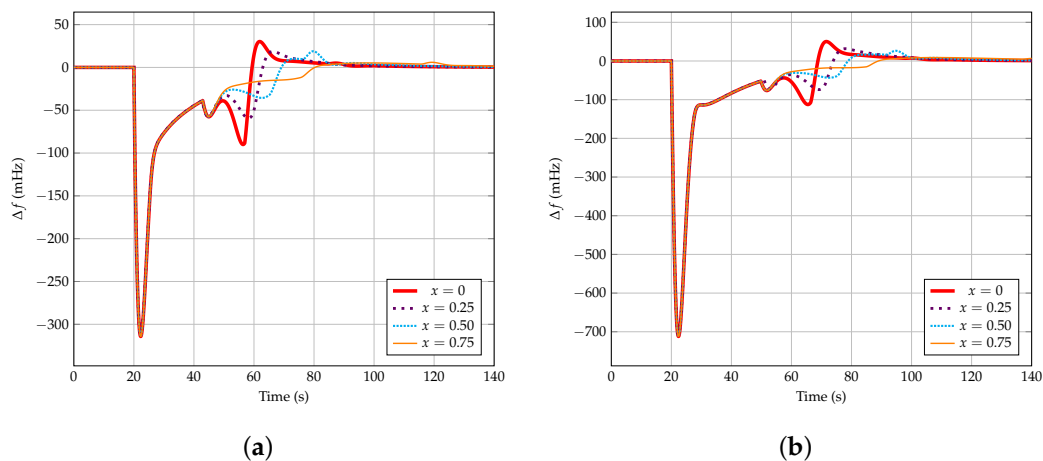

Figure 14. Frequency excursion for scenario 2. Comparison among values of x. (**a**) Considering $\Delta P_L = 0.050$; (**b**) Considering $\Delta P_L = 0.100$.

Figures 15–17 summarize the different scenarios including frequency response from VSWTs when $\Delta P_L = 0.025$, $\Delta P_L = 0.050$ and $\Delta P_L = 0.100$, respectively. Figures 15a, 16a and 17a refer to the controller indicated in [23]. Figures 15b, 16b and 17b use the new proposal of this work, assuming $x = 0.75$ in line with the previous discussion. According to the results, scenarios 2–4 present two different well-identified frequency shifts: (i) due to the power imbalance and (ii) due to the supply-side decrease as a consequence of the step from overproduction to recovery operation mode of the VSWTs frequency controller, see Figure 8.
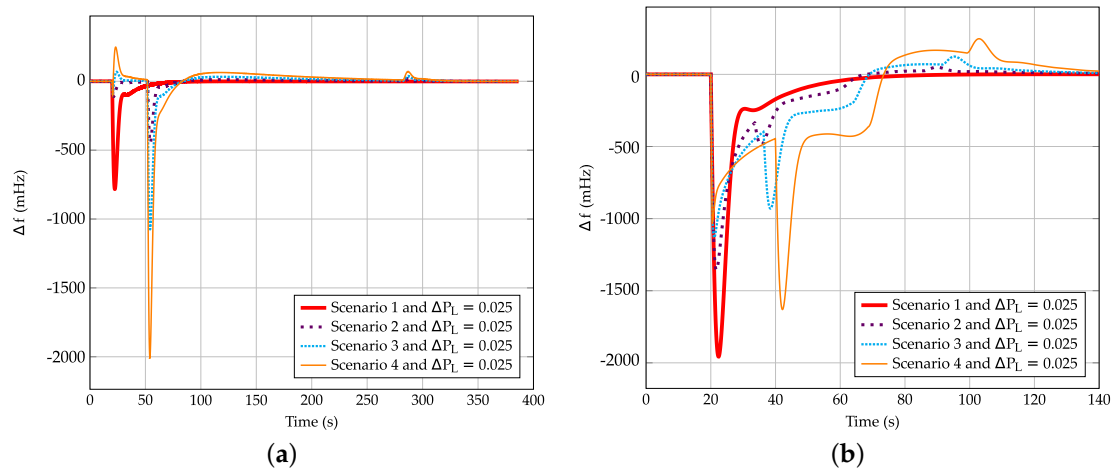
Figure 15. Comparison between frequency excursion for scenarios 1–4 including wind power plant controls and considering $\Delta P_L = 0.025$. (**a**) Controller from [23]; (**b**) Proposed control with $x = 0.75$.

Figure 16. Comparison between frequency excursion for scenarios 1–4 including wind power plant controls and considering $\Delta P_L = 0.050$. (**a**) Controller from [23]; (**b**) Proposed control with $x = 0.75$.
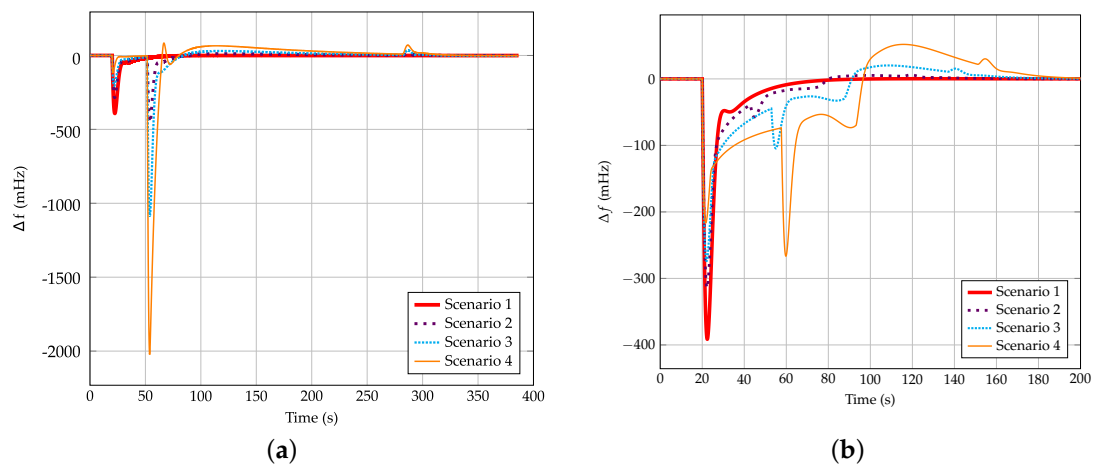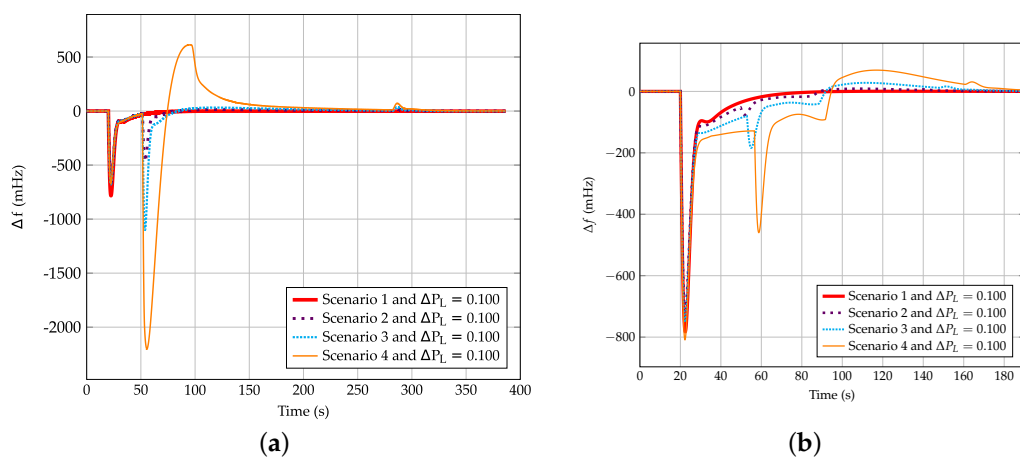

Figure 17. Comparison between frequency excursion for scenarios 1–4 including wind power plant controls and considering $\Delta P_L = 0.100$. (**a**) Controller from [23]; (**b**) Proposed control with $x = 0.75$.

With regard to the power imbalance condition, the frequency shift decreases as the wind energy integration increases. This reduction is due to the fast support provided by VSWTs under a generation-load mismatch. It is more noticeable when the proposal of [23] is considered, as the overproduction power is constant and independent from the frequency deviation. Actually, if the demand variation is small (i.e., $\Delta P_L = 0.025$), the overproduction mode of the approach indicated in [23] may cause an overfrequency instead of an underfrequency, since the additional active power definition ΔP_{OP} (see Figure 15a, scenarios 3 and 4). This drawback does not occur if the adaptive frequency controller proposed in this work is used, as seen in Figure 15b. Considering the case in which $\Delta P_L = 0.050$, a reduction of 70% is obtained with the approach of [23], from 391 mHz in the first scenario to 117 in the last one. This reduction accounts for the 44%, reaching 215 mHz in scenario 4 with the new controller proposal. Finally, when $\Delta P_L = 0.100$, both frequency controllers have similar responses during the firsts seconds, reaching a Nadir $\simeq$ 750 mHz.

With respect to the second frequency shift, it increases with high wind power plant integration, as it increase leads to a greater wind power generation reduction when switching from overproduction to recovery. The underfrequency value can decrease to 2 Hz in scenario 4 with the approach indicated in [23], due to the sudden drop of generation from VSWTs, see Figure 9. Nevertheless, this second excursion is reduced using the smooth recovery proposal of this work, decreasing up to 163, 266, 450 mHz for scenario 4 when $\Delta P_L = 0.025$, $\Delta P_L = 0.050$, $\Delta P_L = 0.100$, respectively. This fact brings out that the new proposed adaptive and smoother controller gives an improvement of the frequency response, being suitable for power systems with high wind power penetration. In Figure 18, a comparison between both frequency deviations corresponding to both frequency control strategies considering $\Delta P_L = 0.050$ are depicted.
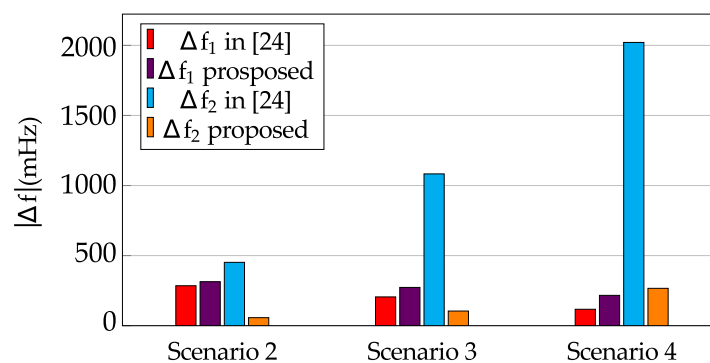

Figure 18. Comparison between Δf_1 and Δf_2 for the different scenarios depending on the wind power plant control and considering $\Delta P_L = 0.050$.

Regarding to ROCOF, its behavior depends on the scenario and ΔP_L. In general, it can be said that ROCOF decreases in scenarios 2 and 3, but increases in scenario 4. Actually, it is higher than the ROCOF of scenario 1 when the wind power plant frequency controller of [23] is analyzed. The stabilization time increases with the wind power plant integration, as a result of the second frequency dip. In the last scenario, the stabilization time is around 280 s for the control strategy indicated in [23] (independently from the value of ΔP_L), varying between 80 and 140 s for the proposed approach. Figures 19 and 20 compare Nadir, stabilization time and Nadir for $\Delta P_L = 0.050$. The increasing of the stabilization time in [23] is due to the fact that when the wind power plant changes from recovery to normal operation mode, a third frequency shift occurs. Despite it is not so noticeable compared to the second frequency excursion, see Figures 15a, 16a and 17a, it can achieve up to 70 mHz for scenario 4.
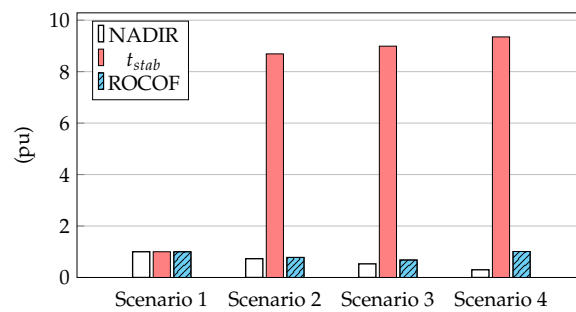
Figure 19. Nadir, stabilization time and ROCOF: comparison for the different scenarios considering $\Delta P_L = 0.050$ and including wind power plant control from [23].
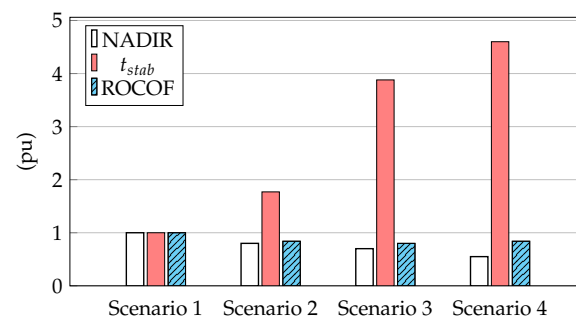

Figure 20. Nadir, stabilization time and ROCOF: comparison for the different scenarios considering $\Delta P_L = 0.050$ and including the proposed wind power plant control.

In Figure 21 the wind power plant response of scenario 2 and $\Delta P_L = 0.050$ with the frequency controller of [23] is depicted. Between points [1]–[2], the VSWT is working in the normal operation mode, providing its maximum power $P_{MPPT} = 0.745$ pu. Because of that, the variation of active power provided is 0 (see definition of ΔP_{WF} in Section 2). The rotational speed of the machine is $\Omega_{MPPT} = 1.197$ pu. At time $t = 20$ s, the power imbalance occurs, activating the overproduction mode (points [2]–[3]). Hence, the variation of active power provided by the wind power plant is constant and equal to $\Delta P_{WF} = 0.1$ pu. This value corresponds to the additional active power provided by the VSWTs in this operation mode, ΔP_{OP}, which is taken from the stored kinetic energy of the machine. As a consequence, the rotational speed of the VSWT decreases from $\Omega_{MPPT} = 1.197$ to the minimum value $\Omega_{WT,min} = 0.700$ pu, corresponding to a 42% of decrease in 30 s. When Ω_{WT} reaches its minimum value, the frequency controller changes to recovery operation mode (points [4]–[5])). The sudden drop of the variation of active power generated (points [3]–[4]) causes a second frequency departure, being this deeper than that due to the power imbalance. This power variation is $\Delta P_{WF} = P_{[4]} - P_{[3]} = -0.27 - 0.1 = -0.37$ pu. Apart from that, it is important to notice that it takes around 250 s to restore the rotational speed to the initial value Ω_{MPPT}.

Regarding to Figure 22, the wind power plant response of scenario 2 and $\Delta P_L = 0.050$ with the proposed controller considering $x = 0.75$ is shown. In this case, the rotational speed decreases from 1.197 to 1.117 pu in 20 s (points [2]–[3]). Despite it takes less time than in Figure 21, the reduction of rotational speed is also lower, only 0.07%. Furthermore, the second frequency departure caused by the drop from overproduction to recovery (points [3]–[4]: $\Delta P_{WF} = P_{[4]} - P_{[3]} = -0.015 - 0.075 = -0.090$ pu) is negligible in comparison to the one indicated in Figure 21. The wind power plant needs only 80 s to restore the rotational speed to the initial value (points [4]–[5]). The equation of the parabola in this case is: $P_{cmd} = 19.06 \cdot \Omega_{WT}^2 - 43.93 \cdot \Omega_{WT} + 26.02$.
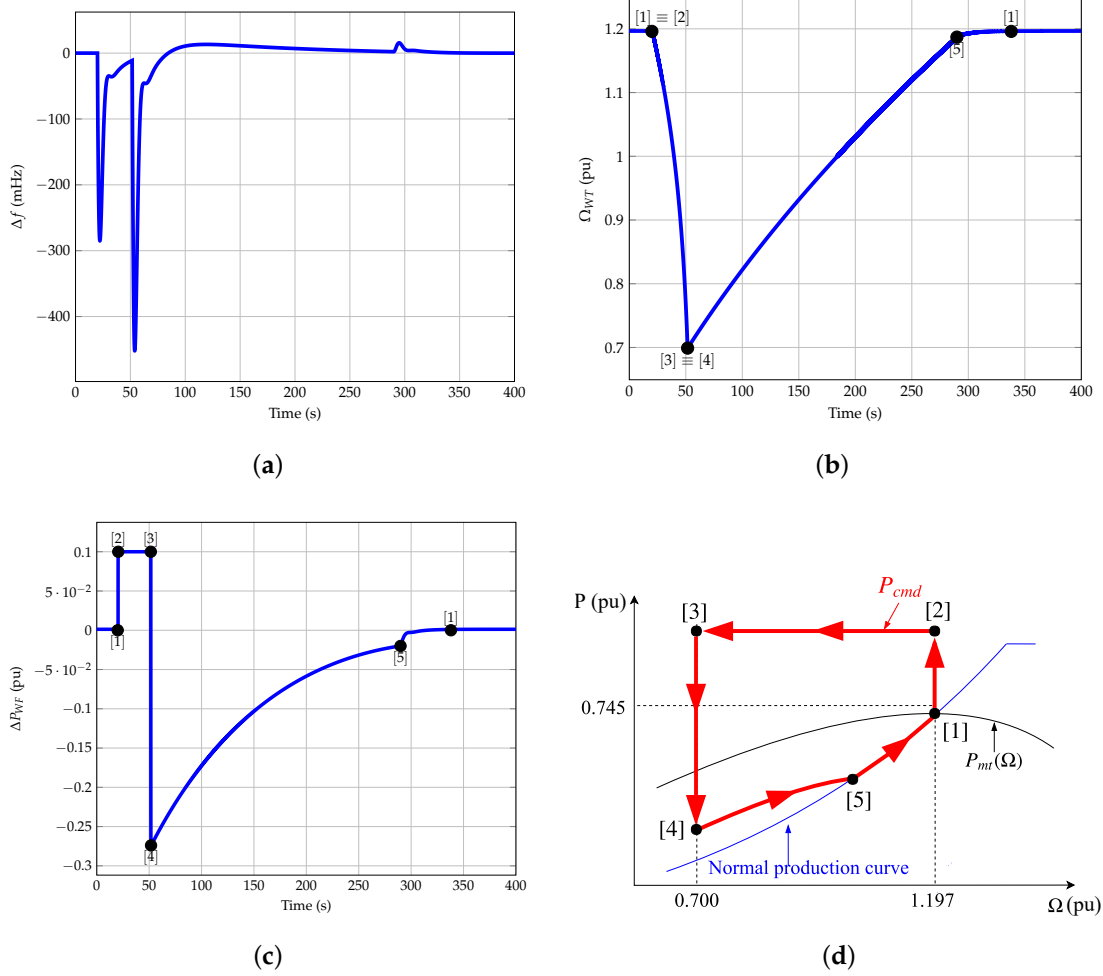
Figure 21. Wind power plant response for scenario 2 and frequency controller of [23]. (**a**) Frequency deviation; (**b**) Rotational speed; (**c**) Variation of wind power; (**d**) Frequency control strategy.
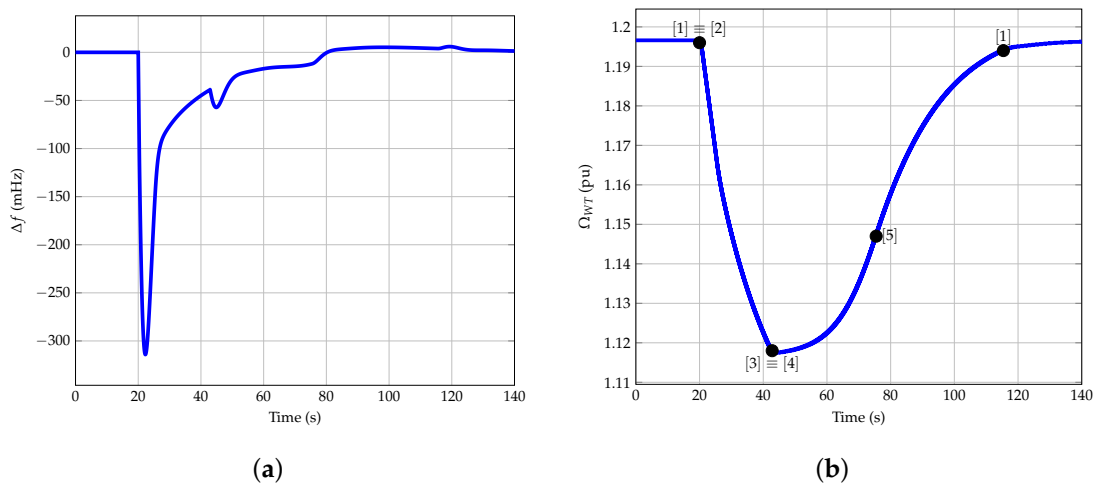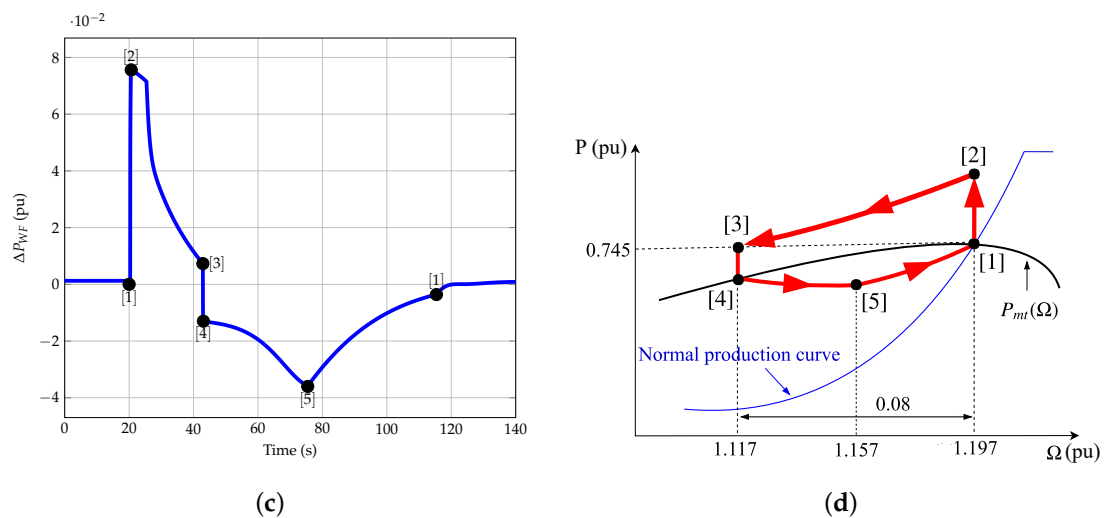

Figure 22. *Cont.*

Figure 22. Wind power plant response for scenario 2 and adaptive and smoother frequency controller with $x = 0.75$. (**a**) Frequency deviation; (**b**) Rotational speed; (**c**) Variation of wind power; (**d**) Frequency control strategy.

5. Conclusions

A new control for VSWTs has been proposed in order to allow them to participate in frequency control. It is based on two operation modes: overproduction and recovery, varying the active power provided by the VSWTs through the 'hidden' kinetic inertia stored in their rotating masses. It is tested within four different supply-side scenarios consisting of thermal, hydro-power and wind power plants. In each scenario, wind power plants have increased their capacity from 15 to 45%, at the time that thermal plants have decreased from 73 to 43% in order to estimate the frequency response of a future power system with high integration of renewable energy sources.

Results show that the Nadir can be reduced a 45% if the wind power plant control proposed participates in frequency control, compared to current situations in which only conventional plants provide frequency control. A secondary frequency dip is identified due to the change from overproduction to recovery periods, consequently increasing the stabilization time. Results are also compared to a previous proposal, improving Nadir, stabilization time and especially the secondary frequency excursion. Actually, it is due to the lack of coordination between power plants, as well as the different time response of the supply-side operation units. New aggregated and coordinated strategies are being analyzed by the authors to minimize the impact of these secondary deviations.

Author Contributions: All authors contributed equally to this work.

Conflicts of Interest: The authors declare no conflict of interest.

Abbreviations

The following abbreviations are used in this manuscript:

a	First parameter of the parabola
b	Second parameter of the parabola
c	Third parameter of the parabola
n	Number of VSWT in the wind power plant
C_P	Power coefficient
D_{eq}	Equivalent damping factor of the power system

H_{eq}	Equivalent inertia constant of the power system
H_i	Inertia constant of each generator unit
P_{acc}	Acceleration power
P_{cmd}	Commanded power of the VSWT
P_e	Active power provided by the wind power plant
P_{ef}	Active measured power provided by the wind power plant
P_{MPPT}	Maximum power point tracking of the VSWT
P_{mt}	Mechanical power of the VSWT
P_1	First point to calculate the parabola: $P_1 : (\Omega_{WT,min}, P_{mt}(\Omega_{WT,min}))$
P_2	Second point to calculate the parabola: $P_2 : (\Omega_V, P_{MPPT}(\Omega_V))$
P_3	Third point point to calculate the parabola: $P_3 : (\Omega_{MPPT}, P_{MPPT}(\Omega_{MPPT}))$
S_B	Rated power of the power system
$S_{B,i}$	Rated power of each power generation unit
V_W	Wind speed
β	Pitch angle
Δf	Frequency excursion
Δf_{lim}	Value at which frequency controller of the VSWT activates
ΔP_g	Variation of active power of the power system: $\Delta P_g = \Delta P_{WF} + \Delta P_T + \Delta P_H$
ΔP_H	Variation of active power of the hydro-power plant
ΔP_L	Variation of power demand
ΔP_{OP}	Additional active power in overproduction operation mode
ΔP_T	Variation of active power of the thermal plant
ΔP_{WF}	Variation of active power of the wind power plant
$\Delta \Omega$	Rotational speed deviation: $\Delta \Omega = \Omega_{MPPT} - \Omega_{WT,min}$
λ	Tip speed ratio
Ω_{err}	Rotational speed error: $\Omega_{err} = \Omega_{WT} - \Omega_{ref}$
Ω_{WT}	Rotational speed of the VSWT
$\Omega_{WT,min}$	Minimum rotational speed of the VSWT
Ω_{MPPT}	Rotational speed at maximum power point tracking
Ω_{ref}	Rotational reference speed
Ω_V	Middle value between $\Omega_{WT,min}$ and Ω_{MPPT}: $\Omega_V = \Omega_{WT,min} + 0.5 \cdot \Delta \Omega$

Appendix A. Parameters for Simulations

Tables A1 and A2 summarize the thermal and hydro-power plant parameters.

Table A1. Thermal power plant parameters [26].

Parameter	Name	Value (pu$_{\text{thermal}}$)
T_G	Speed relay pilot valve	0.20
F_{HP}	Fraction of power generated by high pressure section	0.30
T_{RH}	Time constant of reheater	7.00
T_{CH}	Time constant of main inlet volumes and steam chest	0.30
R_T	Speed droop	0.05
$I(s)$	Integral controller	1.00
$H_{thermal}$	Inertia constant	5.00 s

Table A2. Hydro-power plant parameters [26].

Parameter	Name	Value (pu_{hydro})
T_G	Speed relay pilot valve	0.20
T_R	Reset time	5.00
R_T	Temporary droop	0.38
R_P	Permanent droop	0.05
T_W	Water starting time	1.00
R_H	Speed droop	0.05
$I(s)$	Integral controller	1.00
H_{hydro}	Inertia constant	3.00 s

Appendix B. Wind Turbine Model

The wind turbine model is based on [29,30]. Parameters of the wind turbine model are summarized in Table A4 The mechanical power P_{mt} is obtained (in pu) from

$$P_{mt} = \frac{0.5}{S_n} \cdot C_P \cdot \rho \cdot A_r \cdot V_W^3, \tag{A1}$$

being S_n the rated power, ρ the air density, A_r the swept area by the blades, C_P the power coefficient and V_W the wind speed. The power coefficient C_P is estimated by

$$C_P(\lambda, \beta) = \sum_{i=0}^{4} \sum_{j=0}^{4} \alpha_{i,j} \beta^i \lambda^j. \tag{A2}$$

This expression gives the mathematical representation of the C_P curves, depending on the pitch angle β and the tip speed ratio λ,

$$\lambda = \frac{\Omega_0 \cdot R \cdot \Omega_{WT}}{V_W}, \tag{A3}$$

where Ω_0 is the rotor base speed (rad/s), Ω_{WT} refers to the rotor speed (pu), R is the rotor radius (m) and V_W is the wind speed (m/s). Coefficients of $\alpha_{i,j}$ are taken from Table A3.

Table A3. Coefficients $\alpha_{i,j}$ to calculate $C_P(\lambda, \beta)$

ij	0	1	2	3	4
0	$-4.19 \cdot 10^{-1}$	$2.18 \cdot 10^{-1}$	$-1.24 \cdot 10^{-2}$	$-1.34 \cdot 10^{-4}$	$1.15 \cdot 10^{-5}$
1	$-6.76 \cdot 10^{-2}$	$6.04 \cdot 10^{-2}$	$-1.39 \cdot 10^{-2}$	$1.07 \cdot 10^{-3}$	$-2.39 \cdot 10^{-5}$
2	$1.57 \cdot 10^{-2}$	$-1.01 \cdot 10^{-2}$	$2.15 \cdot 10^{-3}$	$-1.49 \cdot 10^{-4}$	$2.79 \cdot 10^{-6}$
3	$-8.60 \cdot 10^{-4}$	$5.71 \cdot 10^{-4}$	$-1.05 \cdot 10^{-4}$	$5.99 \cdot 10^{-6}$	$-8.91 \cdot 10^{-8}$
4	$1.48 \cdot 10^{-5}$	$-9.48 \cdot 10^{-6}$	$1.62 \cdot 10^{-6}$	$-7.15 \cdot 10^{-8}$	$4.97 \cdot 10^{-10}$

The reference rotational speed Ω_{ref} is estimated from the maximum power tracking based on the measured active power P_{ef}

$$\Omega_{ref} = -0.67 \cdot P_{ef}^2 + 1.42 \cdot P_{ef} + 0.51, \tag{A4}$$

being P_{ef} the active power generated P_e after a delay T_f.

The rotational speed of the wind turbine Ω_{WT} is determined from

$$\Omega_{WT}(s) = \frac{P_e(s) - P_{mt}(s)}{2H_{WT} \cdot s}, \tag{A5}$$

being H_{WT} the inertia constant of the wind turbine. The speed controller is modeled as a PI controller, based on the rotational speed error Ω_{err}

$$T_{cmd_{\Omega_{err}}} = \left(K_{pt} + \frac{K_{it}}{s} \right) \Omega_{err} \tag{A6}$$

Table A4. Wind power plant parameters [29].

Parameter	Name	Value (pu$_{\mathbf{WF}}$)
V_w	Wind speed	10.000 m/s
H_{WT}	Inertia constant	5.190 s
Ω_0	Base rotational speed	1.335 rad/s
T_f	Time delay to measure P_e	5.000 s
T_{con}	Time delay to generate the current I_{inj}	0.020 s
V_{WT}	Wind turbine voltage	1.00
K_{pt}	Proportional constant of speed controller	3.000
K_{it}	Integral constant of speed controller	0.600

References

1. Huber, M.; Dimkova, D.; Hamacher, T. Integration of wind and solar power in Europe: Assessment of flexibility requirements. *Energy* **2014**, *69*, 236–246. [CrossRef]
2. Tselepis, S.; Nikoletatos, J. *Renewable Energy Integration in Power Grids*; The International Renewable Energy Agency: Masdar City, United Arab Emirates, 2015.
3. Bevrani, A.G.H.; Ledwich, G. Renewable energy sources and frequency regulation: Survey and new perspectives. *IET Renew. Power Gener.* **2010**, *4*, 438–457. [CrossRef]
4. Bahrami, S.; Amini, M.H. A decentralized trading algorithm for an electricity market with generation uncertainty. *Appl. Energy* **2018**, *218*, 520–532. [CrossRef]
5. Zhang, W.; Fang, K. Controlling active power of wind farms to participate in load frequency control of power systems. *IET Gener. Transm. Distrib.* **2017**, *11*, 2194–2203. [CrossRef]
6. Shah, R.; Mithulananthan, N.; Bansal, R.; Ramachandaramurthy, V. A review of key power system stability challenges for large-scale PV integration. *Renew. Sustain. Energy Rev.* **2015**, *41*, 1423–1436. [CrossRef]
7. Du, P.; Matevosyan, J. Forecast system inertia condition and its impact to integrate more renewables. *IEEE Trans. Smart Grid* **2018**, *9*, 1531–1533. [CrossRef]
8. Li, D.Y.; Li, P.; Cai, W.C.; Song, Y.D.; Chen, H.J. Adaptive Fault Tolerant Control of Wind Turbines with Guaranteed Transient Performance Considering Active Power Control of Wind Farms. *IEEE Trans. Ind. Electron.* **2017**, *65*, 3275–3285. [CrossRef]
9. Bao, Y.; Xu, J.; Liao, S.; Sun, Y.; Li, X.; Jiang, Y.; Ke, D.; Yang, J.; Peng, X. Field Verification of Frequency Control by Energy-Intensive Loads for Isolated Power Systems with High Penetration of Wind Power. *IEEE Trans. Power Syst.* **2018**, *1*. [CrossRef]
10. Toulabi, M.; Bahrami, S.; Ranjbar, A.M. An Input-to-State Stability Approach to Inertial Frequency Response Analysis of Doubly-Fed Induction Generator-Based Wind Turbines. *IEEE Trans. Energy Convers.* **2017**, *32*, 1418–1431. [CrossRef]

11.   Ochoa, D.; Martinez, S. Proposals for Enhancing Frequency Control in Weak and Isolated Power Systems: Application to the Wind-Diesel Power System of San Cristobal Island-Ecuador. *Energies* **2018**, *11*, 910. [CrossRef]

12.   Aho, J.; Buckspan, A.; Laks, J.; Fleming, P.; Jeong, Y.; Dunne, F.; Churchfield, M.; Pao, L.; Johnson, K. A tutorial of wind turbine control for supporting grid frequency through active power control. In Proceedings of the 2012 American Control Conference (ACC), Montreal, QC, Canada, 27–29 June 2012; pp. 3120–3131. [CrossRef]

13.   Kayikçi, M.; Milanovic, J.V. Dynamic contribution of DFIG-based wind plants to system frequency disturbances. *IEEE Trans. Power Syst.* **2009**, *24*, 859–867. [CrossRef]

14.   Toulabi, M.; Bahrami, S.; Ranjbar, A.M. Application of Edge theorem for robust stability analysis of a power system with participating wind power plants in automatic generation control task. *IET Renew. Power Gener.* **2017**, *11*, 1049–1057. [CrossRef]

15.   Yingcheng, X.; Nengling, T. Review of contribution to frequency control through variable speed wind turbine. *Renew. Energy* **2011**, *36*, 1671–1677. [CrossRef]

16.   Sun, D.; Sun, L.; Wu, F.; Zu, G. Frequency Inertia Response Control of SCESS-DFIG under Fluctuating Wind Speeds Based on Extended State Observers. *Energies* **2018**, *11*, 830. [CrossRef]

17.   Tavakoli, M.; Pouresmaeil, E.; Adabi, J.; Godina, R.; Catalao, J.P. Load-frequency control in a multi-source power system connected to wind farms through multi terminal HVDC systems. *Comput. Oper. Res.* **2018**, *96*, 305–315. [CrossRef]

18.   Alsharafi, A.S.; Besheer, A.H.; Emara, H.M. Primary Frequency Response Enhancement for Future Low Inertia Power Systems Using Hybrid Control Technique. *Energies* **2018**, *11*, 699. [CrossRef]

19.   El Itani, S.; Annakkage, U.D.; Joos, G. Short-term frequency support utilizing inertial response of DFIG wind turbines. In Proceedings of the 2011 IEEE Power and Energy Society General Meeting, San Diego, CA, USA, 24–29 July 2011; pp. 1–8.

20.   Keung, P.K.; Li, P.; Banakar, H.; Ooi, B.T. Kinetic energy of wind-turbine generators for system frequency support. *IEEE Trans. Power Syst.* **2009**, *24*, 279–287. [CrossRef]

21.   Hansen, A.D.; Altin, M.; Margaris, I.D.; Iov, F.; Tarnowski, G.C. Analysis of the short-term overproduction capability of variable speed wind turbines. *Renew. Energy* **2014**, *68*, 326–336. [CrossRef]

22.   Hafiz, F.; Abdennour, A. Optimal use of kinetic energy for the inertial support from variable speed wind turbines. *Renew. Energy* **2015**, *80*, 629–643. [CrossRef]

23.   Tarnowski, G.C.; Kjar, P.C.; Sorensen, P.E.; Ostergaard, J. Variable speed wind turbines capability for temporary over-production. In Proceedings of the 2009 IEEE Power & Energy Society General Meeting, Calgary, AB, Canada, 26–30 July 2009; pp. 1–7.

24.   Kang, M.; Kim, K.; Muljadi, E.; Park, J.W.; Kang, Y.C. Frequency control support of a doubly-fed induction generator based on the torque limit. *IEEE Trans. Power Syst.* **2016**, *31*, 4575–4583. [CrossRef]

25.   Tielens, P.; Hertem, D.V. Receding Horizon Control of Wind Power to Provide Frequency Regulation. *IEEE Trans. Power Syst.* **2017**, *32*, 2663–2672. [CrossRef]

26.   Kundur, P.; Balu, N.J.; Lauby, M.G. *Power System Stability and Control*; McGraw-hill: New York, NY, USA, 1994; Volume 7.

27.   Margaris, I.D.; Papathanassiou, S.A.; Hatziargyriou, N.D.; Hansen, A.D.; Sorensen, P. Frequency control in autonomous power systems with high wind power penetration. *IEEE Trans. Sustain. Energy* **2012**, *3*, 189–199. [CrossRef]

28.   Pyller, M.; Achilles, S. Aggregated Wind Park Models for Analyzing Power System Dynamics. In Proceedings of the 4th International Workshop on Large-Scale Integration of Wind Power and Transmission Networks for Offshore Wind Farms, Billund, Denmark, 20–21 October 2003.

29.   Ullah, N.R.; Thiringer, T.; Karlsson, D. Temporary primary frequency control support by variable speed wind turbines–Potential and applications. *IEEE Trans. Power Syst.* **2008**, *23*, 601–612. [CrossRef]

30.   Miller, N.W.; Sanchez-Gasca, J.J.; Price, W.W.; Delmerico, R.W. Dynamic modeling of GE 1.5 and 3.6 MW wind turbine-generators for stability simulations. In Proceedings of the 2003 IEEE Power Engineering Society General Meeting (IEEE Cat. No.03CH37491), Toronto, ON, Canada, 13–17 July 2003; Volume 3, pp. 1977–1983.

31. Electricity Statistics 2016 (in GWh). 2017. Available online: http://ec.europa.eu/eurostat/statistics-explained/index.php/File:Electricity_Statistics_2016_(in_GWh)-T1.png (accessed on 1 June 2018).

32. ENTSOE.　Network Code on Load-Frequency Control and Reserves.　2013.　Available online: https://www.entsoe.eu/ (accessed on 1 June 2018).